Archives of Current Research International

18(3): 1-15, 2019; Article no.ACRI.50762
ISSN: 2454-7077

Validating Response of AC Microgrid to Line-to-Line Short Circuit in Islanded Mode Using Dynamic Analysis

Maruf A. Aminu[1*]

[1]*Department of Electrical and Electronics Engineering, Nile University of Nigeria, Abuja, Nigeria.*

Author's contribution

The sole author designed, analyzed, interpreted and prepared the manuscript.

Article Information

DOI: 10.9734/ACRI/2019/v18i330135
Editor(s):
(1) Dr. E. V. C. Sekhara Rao, Assistant Professor, Department of EEE, Chaitanya Bharathi Institute of Technology (CBIT), Hyderabad, India.
Reviewers:
(1) Şükrü KİTİŞ, Dumlupınar University, Turkey.
(2) Jurandyr Santos, Nogueira Federal University of Bahia, Brazil.
Complete Peer review History: http://www.sdiarticle3.com/review-history/50762

Original Research Article

Received 09 May 2019
Accepted 13 August 2019
Published 31 August 2019

ABSTRACT

This paper is presented in an attempt to validate the dynamic response of a microgrid to line-to-line short circuit. The microgrid components include two identical Wind Turbine Generators (WTGs) tied to a 100MVA, 13.8kV utility via a Point of Common Coupling (PCC). The utility-microgrid testbed is modeled in SIMPOWERSystems® using two Doubly-Fed Induction Generators (DFIGs) in the microgrid side. While in islanded operating mode, line-to-line short circuit fault is applied at 6.0s and withdrawn at 8.0s, obtaining a 50.0s dynamic response of the system for different fault locations, under voltage and reactive power control regimes of the wind turbine controller. For measurement purpose, the absolute value of the stator complex voltage is transformed to α, β, γ reference frame. Bidirectional power flow between the two feeders is established in the study. The study also confirms that the microgrid composed of DFIGs offer reactive power management capability, particularly by presenting superior performance when stressed under *Q* control regime than under *V* control regime. Finally, the response of the testbed to line-to-line short circuit has been validated and shown to be consistent with established short circuit theory.

Keywords: Microgrid; dynamic; DFIG; microsource; fault.

**Corresponding author: Email: maruf.aminu@gmail.com;*

ABBREVIATIONS

MS1 : *Microsource 1,*
MS2 : *Microsource 2,*
Feeder-a : *Feeder connected to microsource 1,*
P(W) : *Nominal active power in Watts,*
Q(VAr) : *Nominal reactive power in Volt-Amp reactive*

1. INTRODUCTION

The design and operation of power utility seek to generate, transmit and distribute electric power in sufficiently large quantity and on uninterrupted basis to meet the contemporary and projected future demands of the consumers in a load center. In order to achieve this goal, the system must remain in operation continuously without long downtimes. Practically, achieving this goal requires use of protective devices [1-4]. Protective devices function to achieve the following:

1. Minimize damage and repair costs whenever fault is sensed.
2. Safeguard the system to supply power continuously.
3. Consumer and personnel safety [5-9].

In order to meet above requirements, short circuit analyses are normally performed on the system. The analysis will typically aim to determine the short-circuit rating of the equipment to be purchased, installed and commissioned. Also, equipment manufacturers use the ratings specified by their customers to ensure that their equipment are designed to satisfy client's safety and operational specifications under certain conditions for specified duration [10-13]. As the parameters of a power system and fault envelopes vary with time [14-16], short circuit analysis which depicts the system dynamics is useful in order to achieve the utility operational goals - ensuring high quality, continuous and safe delivery of power to consumers [17-20].

In this work, the author presents a utility-microgrid testbed for a research which aims at proposing a new microgrid protection. Since the protection to be developed would be based on measurement of three-phase power, the nominal three-phase active and reactive power is used and presented in this paper. Thus, this paper presents an attempt to validate the response of the modeled testbed to line-to-line short circuit. This is because the validity of the anticipated protection depends on the validity of the testbed's response to short circuit.

2. SHORT CIRCUIT IN A POWER SYSTEM

Consider a three phase-to-earth fault at point F2 as shown in Fig. 1.

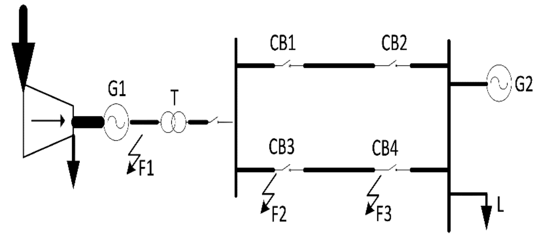

Fig. 1. Typical power system with short circuit points F1, F2 and F3

In an electric power generator, fault current is often initially around 8 times the full-load current. It attenuates rapidly to around 5 times full-load current before attenuating less rapidly to less than full-load current value. In the direct axis, this results in three stages of fault current envelop named sub-transient $(X_d^{''})$, transient $(X_d^{'})$ and steady-state (X_d) respectively.

Fault F2 is therefore seen as a modified generator fault which incorporates the effect of transformer T. The transformer reactance, X_T, is added to the reactances $X_d^{''}$, $X_d^{'}$ and X_d as given in (1), (2) and (3) [4,6,7,20].

$$x_d^{''} = X_d^{''} + X_T \tag{1}$$

$$x_d^{'} = X_d^{'} + X_T \tag{2}$$

$$x_d = X_d + X_T \tag{3}$$

The amplitude of the ac fault current in the sub-transient state, $i_m^{''}$, transient state, $i_m^{'}$, and steady state, i_m^{∞}, is presented in (4), (5) and (6), respectively.

$$i_m^{''} = \frac{E_{fm}}{x_d^{''}} \tag{4}$$

$$i_m^{'} = \frac{E_{fm}}{x_d^{'}} \tag{5}$$

$$i_m^{\infty} = \frac{E_{fm}}{x_d} \tag{6}$$

Addition of X_T attenuates the magnitude of the currents given in (4), (5) and (6). Secondly, the rate of dissipation of the stored magnetic energy is increased by the transformer resistance, R_T, so that the dc component of short circuit current decays more rapidly. Thirdly, the time constants are increased by the transformer reactance as given in (7) and (8) [21-23].

$$T_{d(network)}^{"} = T_d^{"}\left(\frac{X_d^{'}}{X_d^{"}}\right)\left(\frac{X_d^{"}+X_T}{X_d^{'}+X_T}\right) \tag{7}$$

$$T_{d(network)}^{'} = T_d^{'}\left(\frac{X_d}{X_d^{'}}\right)\left(\frac{X_d^{'}+X_T}{X_d+X_T}\right) \tag{8}$$

3. DESIGN OF CONTROL SYSTEMS

The modeled system is subjected to small signal response analysis. It is found to be stable but its response time is unsatisfactory. Requisite regulators are then designed using closed-loop feedback structure. The systems designed are pitch angle regulator, active power management systems and reactive power management systems. The regulators are combined to implement two mutually exclusive control regimes. These two regimes are active power-voltage (*V*) control and reactive-active power (*Q*) control. Under power-voltage control, the controller maintains constant grid voltage with a 4% droop. Under reactive-active power control, the controller ensures constant reactive power at the grid.

4. SHORT CIRCUIT SIMULATION AND SYSTEM DYNAMIC RESPONSE

The testbed developed for this study is shown in Fig. 2. In the network, each DFIG is nominally rated 5.5kW, 575V and linked to 2.5 km highly resistive feeder (a or b). Each feeder is connected to the utility radially at the PCC. A modeled 20MVA STATCOM is connected to the utility side at the PCC. A local inductive load of 3.6MVA and a remote inductive load of 89.44MVA are serviced by the utility. A total inductive local load of 6.21kVA is serviced by the microgrid. The operating frequency of the system is 50Hz, with cut-in and cut-out wind speeds of 3 ms^{-1} and 6 ms^{-1}, respectively. Islanding of the microgrid is achieved by opening the PCC.

Fig. 3 shows the response of MS1 during normal operation under *V* and *Q* controls.

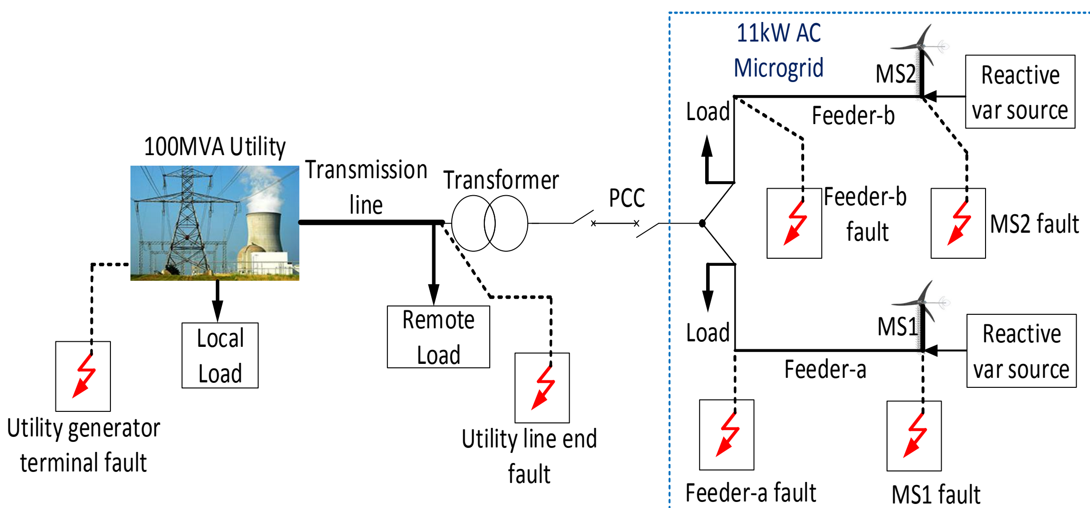

Fig. 2. A basic diagram displaying the system under study

5. LINE-TO-LINE SHORT CIRCUIT

Line-to-line short circuit fault is applied at 6.0s and withdrawn at 8.0s. Under this short circuit, system's (microgrid feeders and DFIG) dynamics is simulated for 50.00s. The testbed's responses for different fault locations and DFIG controller in voltage, *V*, and reactive power, *Q*, control are obtained and presented in Fig. 4 to Fig. 19.

The responses of MS1 to short circuits at the terminals of utility generator under *V* and *Q* controls are presented in Fig. 4 and Fig. 5, respectively.

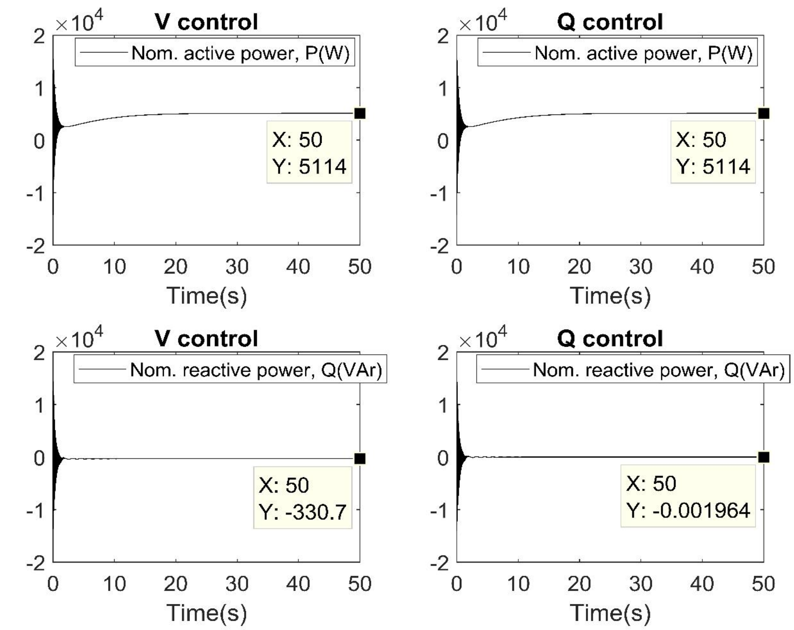

Fig. 3. Response of MS1 under normal operation in *V* and *Q* Controls

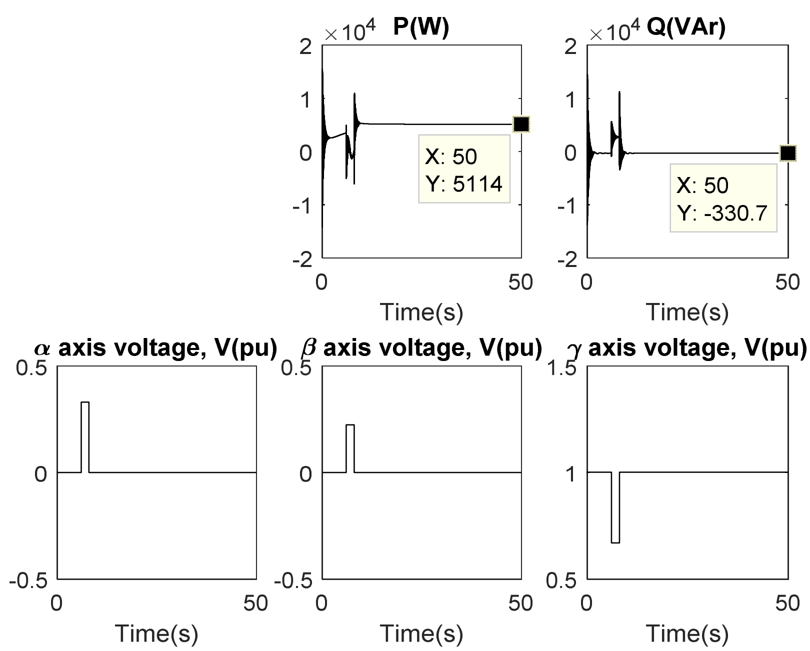

Fig. 4. Response of MS1 to L-L short circuit – *V* control

Fig. 6 shows response of feeder-a to short circuit at terminals of MS1 under *V* control, while Fig. 7 shows response of same feeder to same short circuit under Q control.

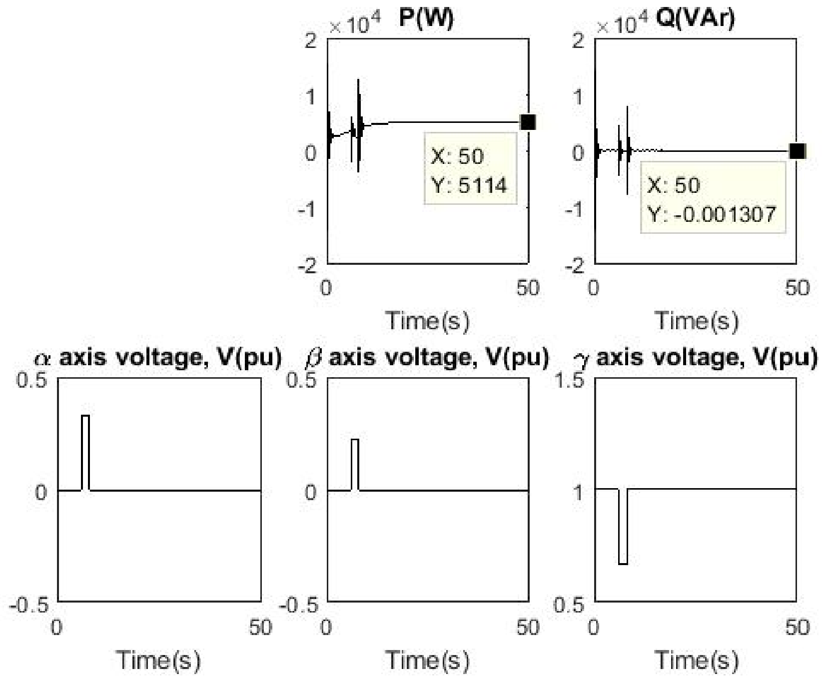

Fig. 5. Response of MS1 to L-L short circuit – Q control

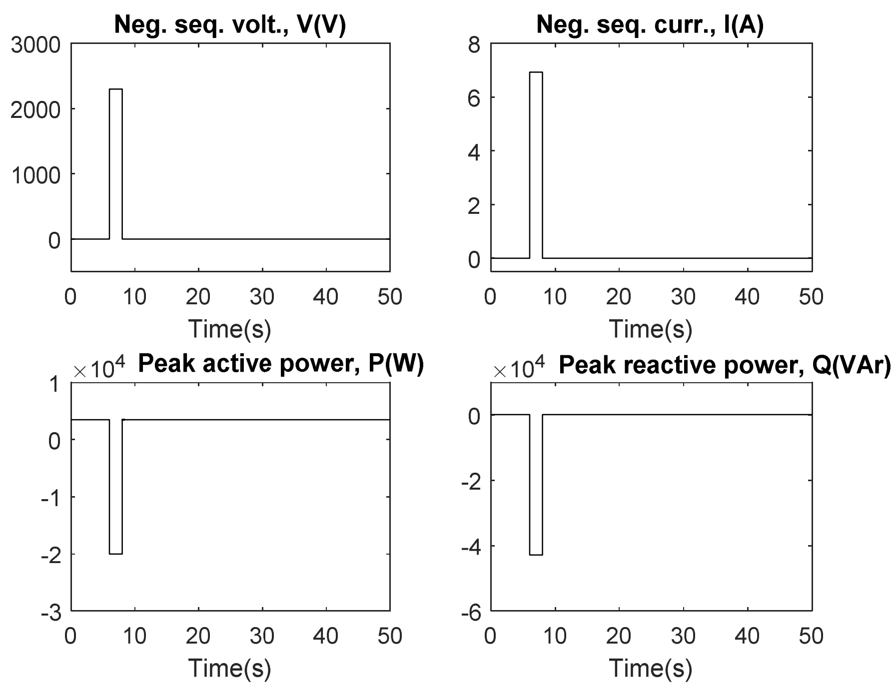

Fig. 6. Response of feeder-a to L-L short circuit at terminals of MS1– V control

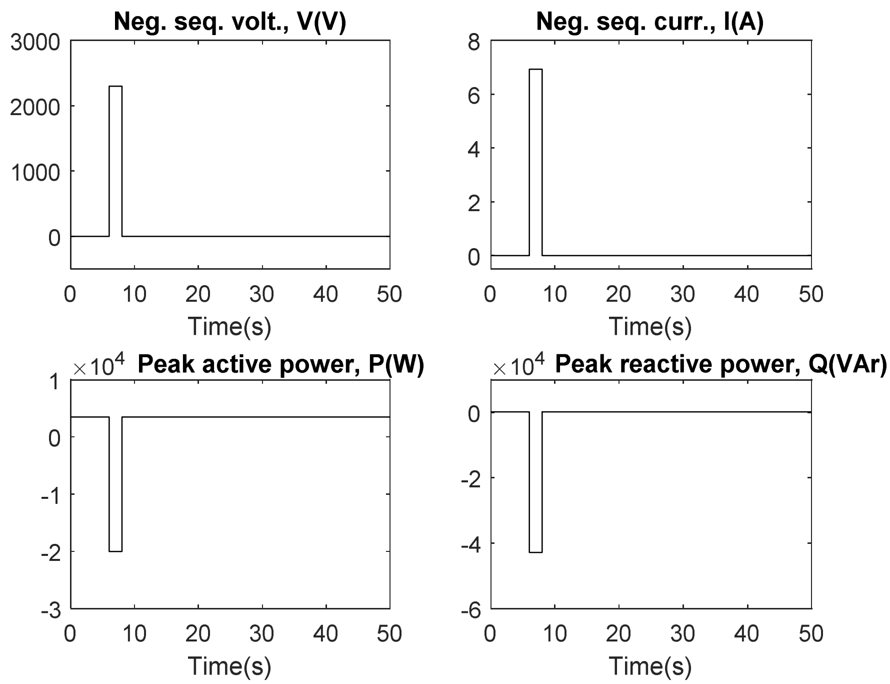

Fig. 7. Response of feeder-a to L-L short circuit at terminals of MS1– Q control

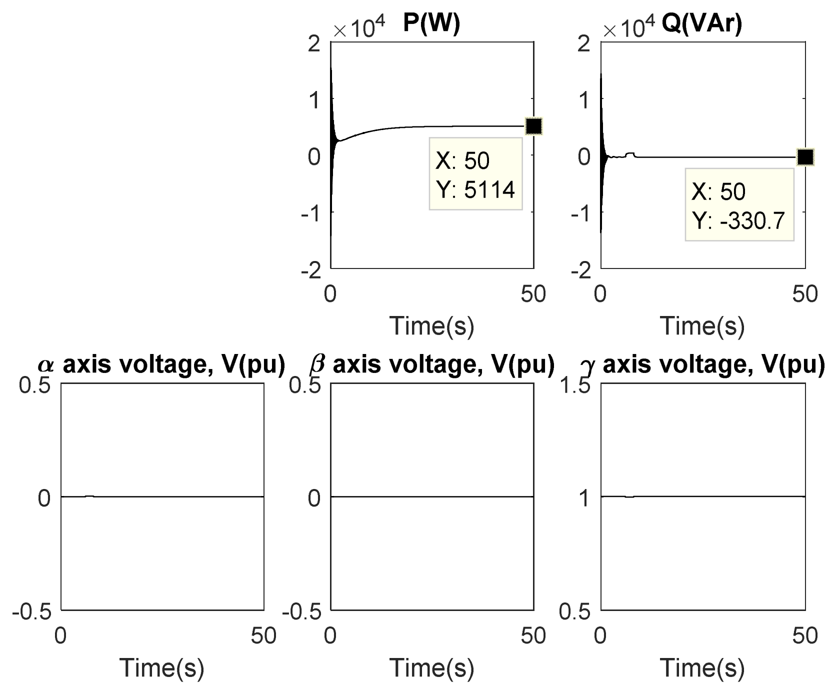

Fig. 8. Response of MS1 to L-L short circuit at ends of feeder-a – *V* control

Note that under *V* control (Fig. 4) when L-L short circuit is applied at its terminals, MS1 absorbs 330.7 VAr from its reactive VAr compensator and that of MS2 at 50.00s. This is considerably higher than 0.001307 VAr it absorbs under *Q* control (Fig. 5), indicative of reactive power management of DFIG as published by Moayed Moghbel et al. in [24] and in [25-27]. The peak active power of feeder-a rose to 20kW in a direction opposite the nominal active power flow direction during the fault, indicating active power support from MS2 and feeder-b to feed the fault point in feeder-a. Similarly, reactive power flow on feeder-a rose to more than 40k VAr in an opposite direction during the fault, as seen in Fig. 6. Negative sequence quantities only exist during the fault, as depicted in Fig. 6 and Fig. 7.

The responses of MS1 to short circuits at the ends of feeder-a under *V* and *Q* controls are presented in Fig. 8 and Fig. 9, respectively.

Fig. 10 shows response of feeder-a when it is short-circuited under *V* control, while Fig. 11 shows response of same feeder to same short circuit under *Q* control.

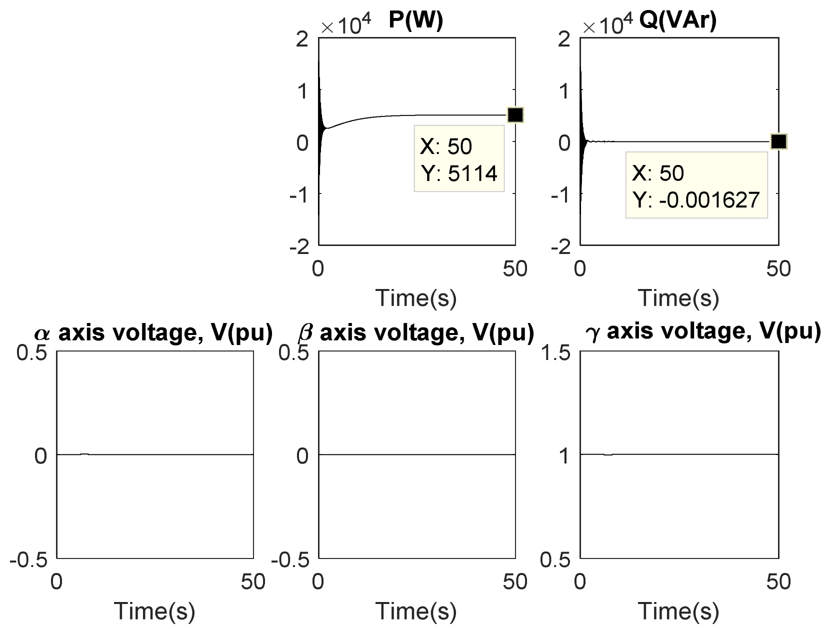

Fig. 9. Response of MS1 to L-L short circuit at ends of feeder-a – *Q* control

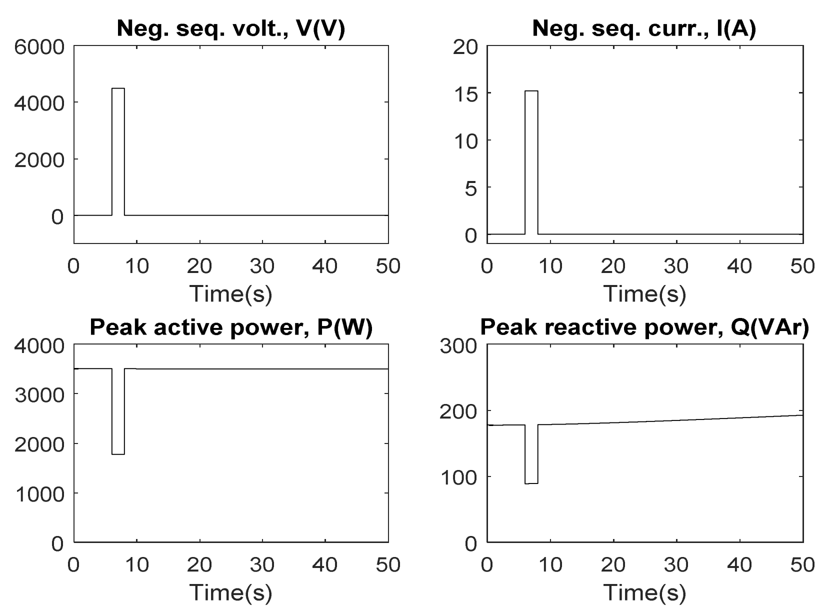

Fig. 10. Response of feeder-a when it is short-circuited – *V* control

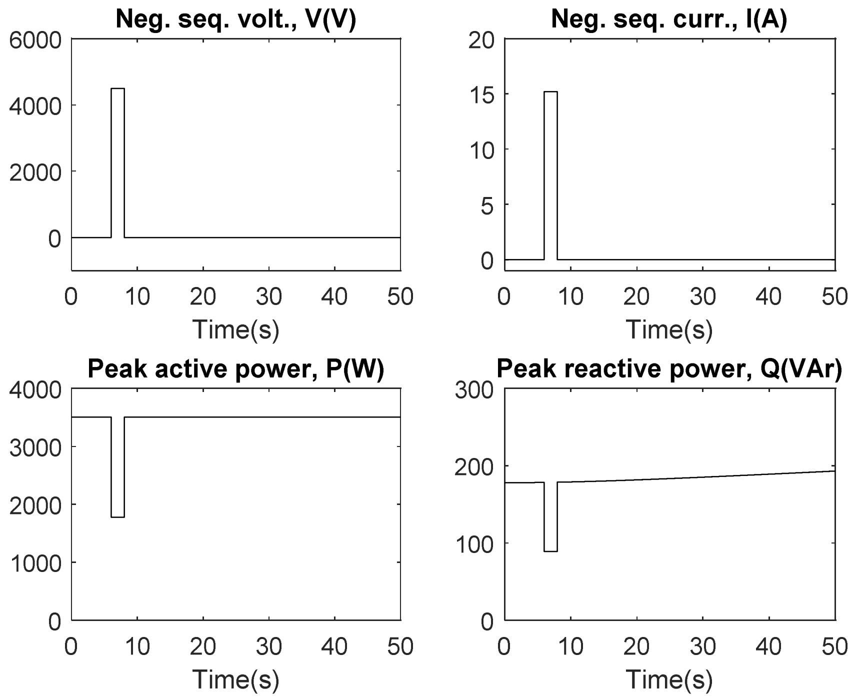

Fig. 11. Response of feeder-a when it is short-circuited – *Q* control

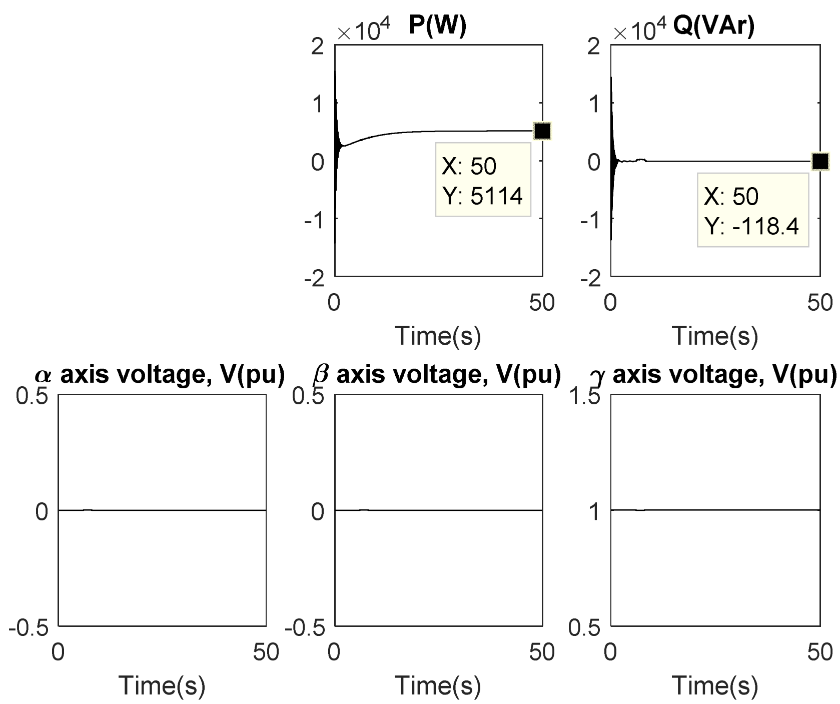

Fig. 12. Response of MS2 to L-L short circuit at terminals of MS1 – *V* control

Fig. 12 shows response of MS2 when terminals of MS1 are short-circuited under *V* control, while Fig. 13 shows response of MS2 when terminals of MS1 are short-circuited under *Q* control.

Fig. 14 shows response of MS2 when ends of feeder-a are short-circuited under *V* control, while Fig. 15 shows response of MS2 when ends of feeder-a are short-circuited under *Q* control.

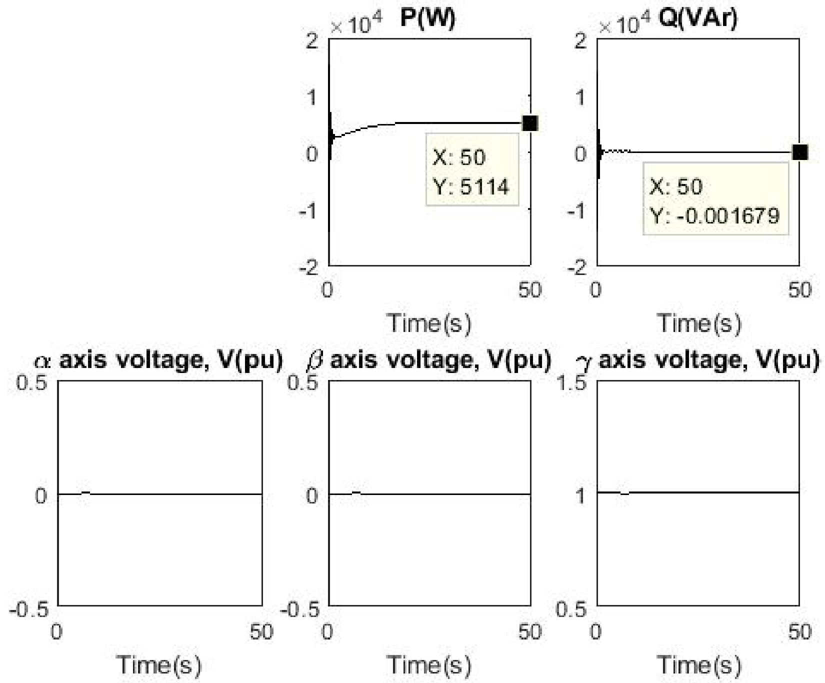

Fig. 13. Response of MS2 to L-L short circuit at terminals of MS1 – *Q* control

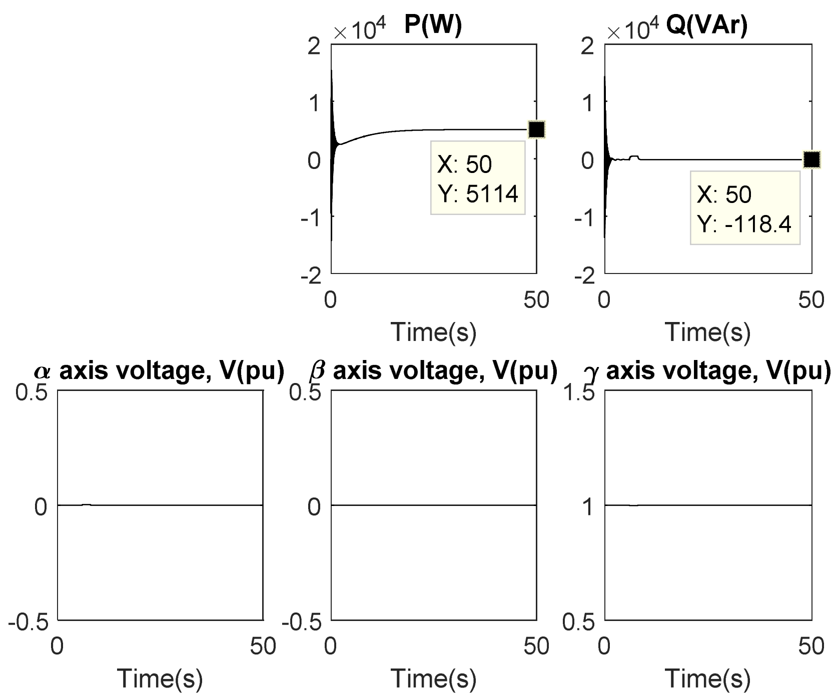

Fig. 14. Response of MS2 to L-L short circuit at ends of feeder-a – *V* control

Fig. 16 shows response of MS1 to cross-country L-L short circuit at terminals of MS1 and MS2 under *V* control, while Fig. 17 shows response of MS1 to same fault as in Fig. 16 but under *Q* control.

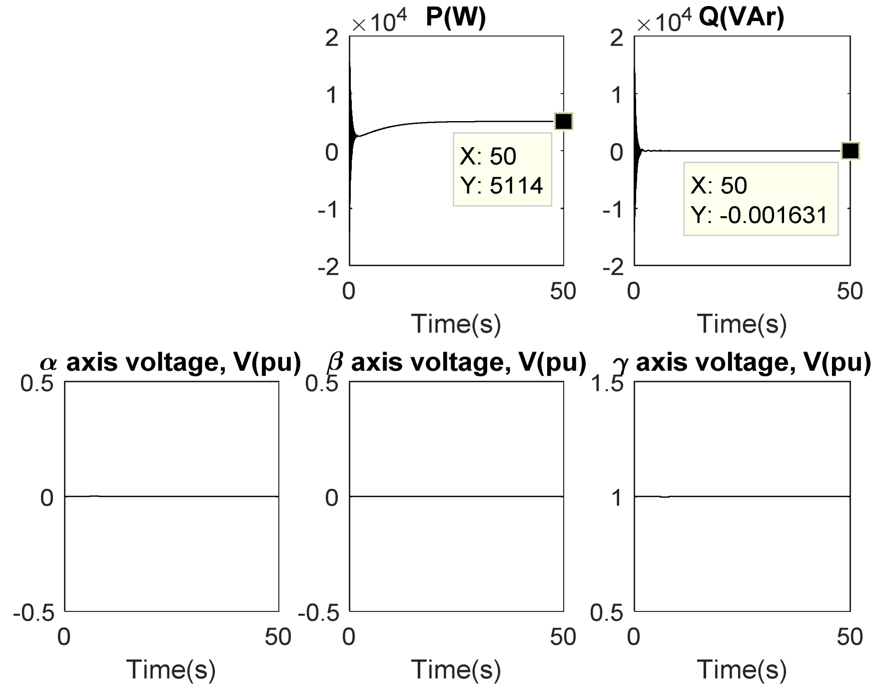

Fig. 15. Response of MS2 to L-L short circuit at ends of feeder-a – *Q* control

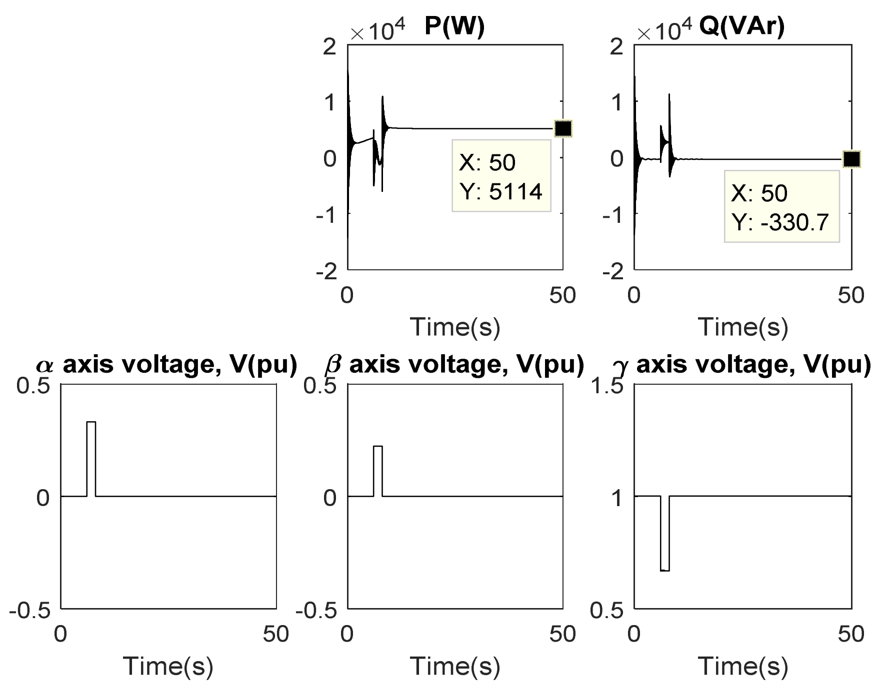

Fig. 16. Response of MS1 to cross-country L-L short circuit at terminals of MS1 and MS2 – *V* control

6. THREE PHASE BOLTED SHORT CIRCUIT

In order to present a peek into the response of the microsource as short circuit severity increases, its response to three phase bolted short circuit is presented in Fig. 18 and Fig. 19.

Fig. 18 and Fig. 19 show response of MS1 when three phase-to-ground bolted short circuit is applied at its terminals under *V* control and *Q* control, respectively.

7. RESULTS AND DISCUSSION

As observed from the simulation results, the generation of each microsource is 92% of its nominal rating when operating under stress-free condition. Similarly, during normal operation, absorption of reactive power of each microsource from the external reactive power compensator is more under *V* control than *Q* control. This indicates DFIG's reactive support from its converter dc bus under *Q* control. This reactive support is, however, unsustainable for continuous operation since the capacitor linked to its converter dc bus is of small capacity.

At 50.0s, under *V* control (Fig. 4) when L-L short circuit is applied at its terminals, MS1 absorbs 330.7 VAr from its reactive VAr compensator and that of MS2. This is considerably higher than 0.001307 VAr it absorbs under *Q* control (Fig. 5), indicative of reactive power management of DFIG as published by Moayed Moghbel et al. in [24] and in [25-27]. The peak active power of feeder-a rose to 20kW in a direction opposite the nominal active power flow direction during the fault, indicating active power support from MS2 and feeder-b to feed the fault point in feeder-a. Similarly, reactive power flow on feeder-a rose to more than 40 kVAr in an opposite direction during the fault, as seen in Fig. 5. Negative sequence quantities only exist during the fault, as depicted in Fig. 6 and Fig. 7.

At 50.0s, under *V* control (Fig. 8) when L-L short circuit is applied at ends of feeder-a, MS1 absorbs 118.4 VAr from the reactive VAr compensators. This is considerably higher than 0.001627 VAr it absorbs under *Q* control (Fig. 9), indicative of reactive power management of DFIG as published by Moayed Moghbel et al. in [24] and in [28,29]. The peak active power of feeder-a dropped to less than 2kW during the fault. Similarly, reactive power flow on feeder-a dropped to less than 100 VAr during the fault, as seen in Fig. 10 and Fig. 11. Negative sequence quantities only exist during the fault, as depicted in Fig. 9 and Fig. 11.

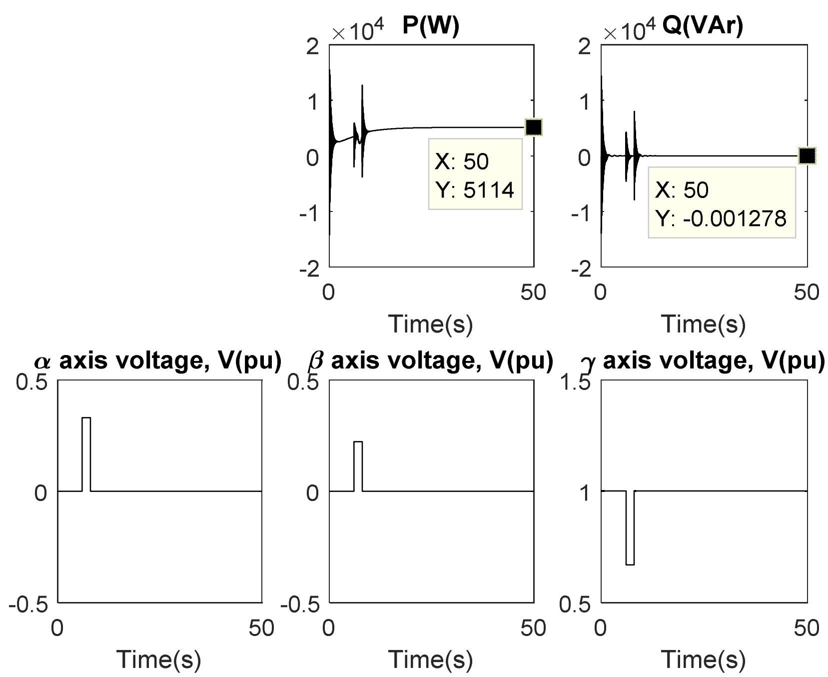

Fig. 17. Response of MS1 to cross-country L-L short circuit at terminals of MS1 and MS2 – *Q* control

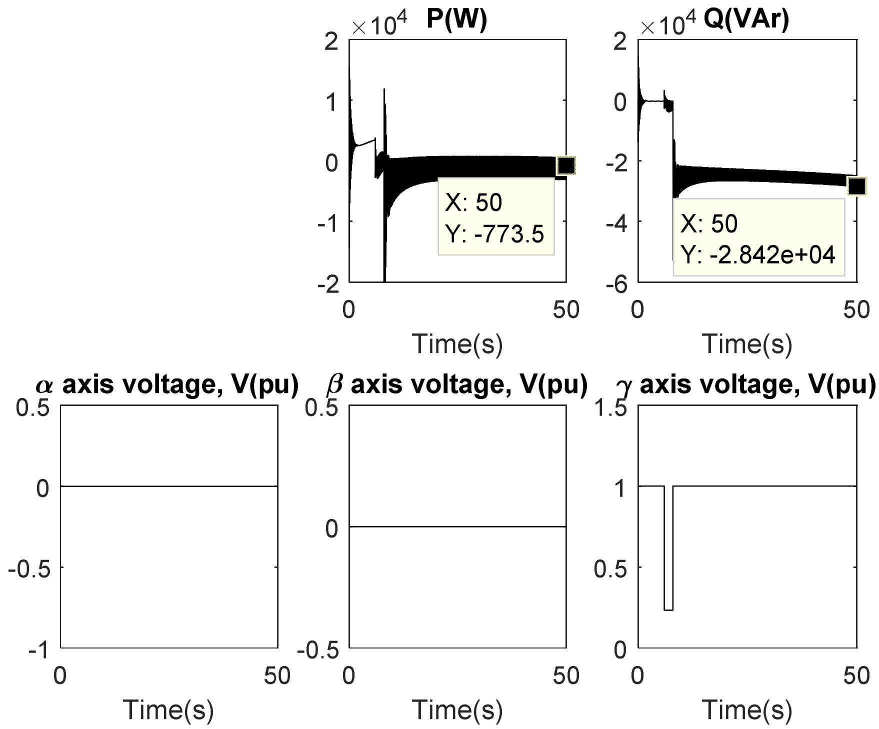

Fig. 18. Response of MS1 to 3-phase bolted short circuit – *V* control

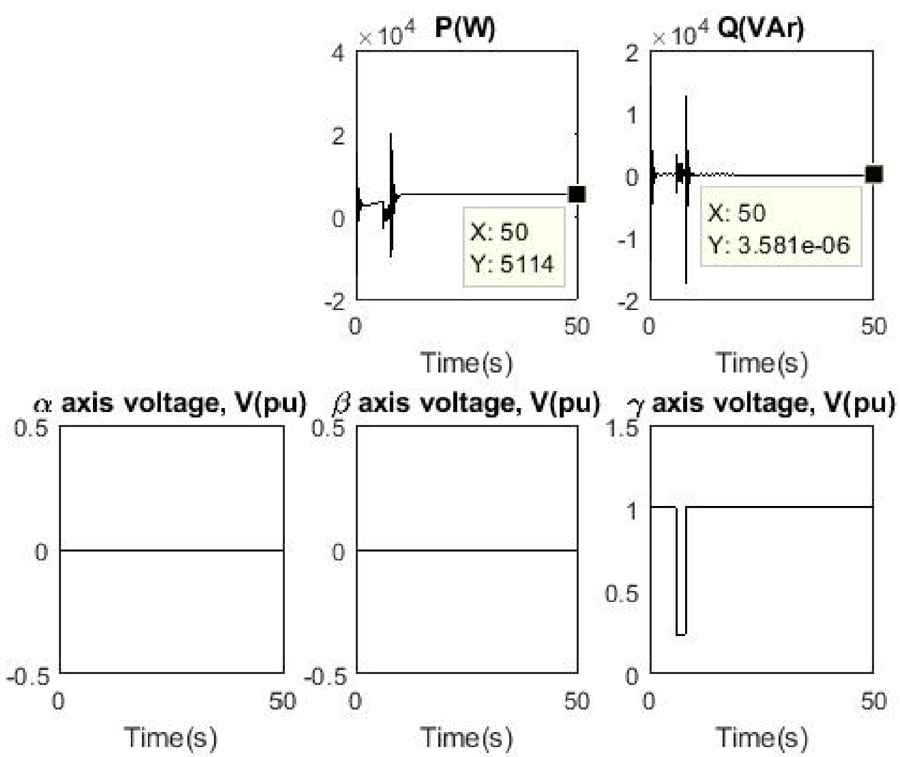

Fig. 19. Response of MS1 to 3-phase bolted short circuit – *Q* control

At 50.0s, under *V* control (Fig. 12) when L-L short circuit is applied at terminals of MS1, MS2 absorbs 118.4 VAr from the reactive VAr compensators. This is considerably higher than 0.001679 VAr it absorbs under *Q* control (Fig. 13), indicating reactive power management of DFIG as published by Moayed Moghbel et al. in [24] and in [28,29]. The transformed stator voltage of MS2 is undisturbed as the severity of the fault is minimized by the impedance of feeder-a and feeder-b, as shown in Fig. 12 to Fig. 15.

At 50.0s, under *V* control (Fig. 16) when cross-country L-L short circuit is applied at terminals of MS1 and MS2, MS1 absorbs 330.7 VAr from the reactive VAr compensators. This is considerably higher than 0.001278 VAr it absorbs under *Q* control (Fig. 17), indicating reactive power management of DFIG as published by Moayed Moghbel et al. in [24] and in [28,29]. Both active and reactive power of MS1 are unstable during the fault in both *V* and *Q* control, but more visible instability is observed under *V* control regime. Voltage and frequency instability is a major challenge of microgrid operation, as published in [30-33]. During the fault, the transformed stator voltages of MS1 is disrupted in the α, β and γ axes as the severity of the fault is higher than L-L faults that are not cross-country, as shown in Fig. 16 and Fig. 17.

At 50.0s, under *V* control (Fig. 18) when 3-phase bolted short circuit is applied at terminals of MS1, MS1 absorbs (a change of operation from generation mode to motoring mode of DFIG) 0.7735kW from MS2 and also absorbs 28.42 kVAr from the reactive VAr compensators. This is considerably higher than under *Q* control regime (Fig. 19) where, with same short circuit, MS1 generates 5.114kW and supports the system with 3.581×10^{-6} VAr. This validates reactive power management of DFIG as published by Moayed Moghbel et al. in [24] and in [28,29]. Both active and reactive power of MS1 are unstable during the fault in both *V* and *Q* control, but virulent and sustained instability is observed under *V* control regime. Voltage and frequency instability is a major challenge of microgrid operation, as published in [30-32]. The DFIG remained in generation mode under *Q* control while it changed to motoring mode under *V* control when exposed to 3-phase bolted short circuit. During the fault, the transformed stator voltages of MS1 is disrupted in the γ axis as the severity of the fault is high, as shown in Fig. 18 and Fig. 19.

8. CONCLUSION

The simulation results of this work has shown that when the system is under 2-second line-to-line short circuit stress, bidirectional flow of active and reactive power between the two feeders occurs, particularly power support at fault points. The simulation has also verified the theory of power management capability of DFIG by showing that each microsource offers superior active and reactive power post-fault stability under *Q* control than *V* control when the microgrid is faulted. This is especially obvious as the fault severity increases due to the effect of power electronic (converter and controller) interfacing of DFIG. Finally, the interaction and the engagement of critical quantities in a wind turbine distributed generation with a local load has been explored and depicted. Such is the α, β, γ transformation of DFIG's complex form of stator voltage (a, b, c). Each set of α, β, γ plot shows a unique pattern to fault location, making the α, β, γ transformation a potential candidate for fault sensing and diagnosis – regardless of control regime. In conclusion, the response of the testbed to line-to-line short circuit has been shown to agree with established theory. This helps validate its response to line-to-line short circuit.

COMPETING INTERESTS

Author has declared that no competing interests exist.

REFERENCES

1. Didier G, Bonnard CH, Lubin T, Lévêque J. Comparison between inductive and resistive SFCL in terms of current limitation and power system transient stability. Electric Power Systems Research. 2015;125:150-158.
2. Filipović-Grčić D, Filipović-Grčić B, Capuder K. Modeling of three-phase autotransformer for short-circuit studies. International Journal of Electrical Power & Energy Systems. 2014;56:228-234.
3. Papaefthymiou SV, Lakiotis VG, Margaris ID, Papathanassiou SA. Dynamic analysis of island systems with wind-pumped-

storage hybrid power stations. Renewable Energy. 2015;74:544-554.
4. Sulla F, Svensson J, Samuelsson O. Symmetrical and unsymmetrical short-circuit current of squirrel-cage and doubly-fed induction generators. Electric Power Systems Research. 2011;81:1610-1618.
5. Chen TH, Huang WT. Evaluation of the variations of short-circuit capacities along a feeder due to distribution system-type upgrading. International Journal of Electrical Power & Energy Systems. 2009;31:50-58.
6. Roennspiess OE, Efthymiadis AE. A comparison of static and dynamic short circuit analysis procedures. IEEE Transactions on Industry Applications. 1990;26:463-475.
7. Soni N, Doolla S, Chandorkar MC. Improvement of transient response in microgrids using virtual inertia. IEEE Transactions on Power Delivery. 2013;28: 1830-1838.
8. Palizban O, Kauhaniemi K, Guerrero JM. Microgrids in active network management – part II: System operation, power quality and protection. Renewable and Sustainable Energy Reviews. 2014;36: 440-451.
9. Patrao I, Figueres E, Garcerá G, González-Medina R. Microgrid architectures for low voltage distributed generation. Renewable and Sustainable Energy Reviews. 2015;43:415-424.
10. Adio OS, Xiangning L, Feng Z, Zhiqian B. Short circuit analysis for integration of 10MW Windfarm in Nigeria at the PCC. In: 2013 IEEE Power and Energy Society General Meeting (PES). 2013;1-5.
11. Chaudhary M, Brahma SM, Ranade SJ. Short circuit analysis of type II induction generator and wind farm. In: 2012 IEEE PES Transmission and Distribution Conference and Exposition (T&D). 2012;1-5.
12. Mathur A, Pant V, Das B. Unsymmetrical short-circuit analysis for distribution system considering loads. International Journal of Electrical Power & Energy Systems. 2015;70:27-38.
13. Samaan N, Zavadil R, Smith JC, Conto J. Modeling of wind power plants for short circuit analysis in the transmission network. In: Transmission and Distribution Conference and Exposition. T&D. IEEE/PES. 2008;1-7.
14. Hatziargyriou N, Asano H, Iravani R, Marnay C. Microgrids. IEEE Power and Energy Magazine. 2007;5:78-94.
15. Jan Machowski JWB, James R. Bumby. Power system dynamics and stability. John Wiley & Sons, England; 1997.
16. Lasseter RH. MicroGrids. In: 2002 IEEE Power Engineering Society Winter Meeting. 2002;301:305-308.
17. Best RJ, Morrow DJ, Crossley PA. Current transients in the small salient-pole alternator during sudden short-circuit and synchronisation events. IET Electric Power Applications. 2010;4:687-700.
18. Kersting WH, Shirek G. Short circuit analysis of IEEE test feeders. In: IEEE PES Transmission and Distribution Conference and Exposition (T&D). 2012;1-9.
19. Ouyang J, Xiong X. Research on short-circuit current of doubly fed induction generator under non-deep voltage drop. Electric Power Systems Research. 2014;107:158-166.
20. Prajapati J, Patel V, Patel H. Load flow, short circuit and stability analysis using Matlab. In: Green Computing Communication and Electrical Engineering (ICGCCEE), International Conference on. 2014;1-5.
21. Bracale A, Caramia P, Di Fazio AR, Proto D. Probabilistic short circuit analysis in electric power distribution systems including distributed generation. In: 8th Mediterranean Conference on Power Generation, Transmission, Distribution and Energy Conversion (MEDPOWER 2012). 2012;1-6.
22. Jen-Hao T. Unsymmetrical short-circuit fault analysis for weakly meshed distribution systems. IEEE Transactions on Power Systems. 2010;25:96-105.
23. Ouyang J, Xiong X. Dynamic behavior of the excitation circuit of a doubly-fed induction generator under a symmetrical voltage drop. Renewable Energy. 2014;71: 629-638.
24. Moghbel M, Mokui HT, Masoum MAS, Mohseni M. Reactive power control of DFIG wind power system connected to IEEE 14 bus distribution network. In: Universities Power Engineering Conference (AUPEC), 22nd Australasian. 2012;1-7.
25. Dongliang X, Zhao X, Lihui Y, Ostergaard J, Yusheng X, Kit Po W. A comprehensive

LVRT control strategy for DFIG wind turbines with enhanced reactive power support. IEEE Transactions on Power Systems. 2013;28:3302-3310.
26. Jeong-Ik J, Young-Sin K, Dong-Choon L. Active and reactive power control of DFIG for wind energy conversion under unbalanced grid voltage. In: IEEE 5th International Power Electronics and Motion Control Conference, IPEMC 2006. 2006;1-5.
27. Kayikci M, Milanovic JV. Reactive power control strategies for DFIG-based plants. IEEE Transactions on Energy Conversion. 2007;22:389-396.
28. Gopalan SA, Sreeram V, Iu HHC. A review of coordination strategies and protection schemes for microgrids. Renewable and Sustainable Energy Reviews. 2014;32: 222-228.
29. Planas E, Gil-de-Muro A, Andreu J, Kortabarria I, Martínez de Alegría I. General aspects, hierarchical controls and droop methods in microgrids: A review. Renewable and Sustainable Energy Reviews. 2013;17:147-159.
30. Romo R, Micheloud O. Power quality of actual grids with plug-in electric vehicles in presence of renewables and micro-grids. Renewable and Sustainable Energy Reviews. 2015;46:189-200.
31. Soshinskaya M, Crijns-Graus WHJ, Guerrero JM, Vasquez JC. Microgrids: Experiences, barriers and success factors. Renewable and Sustainable Energy Reviews. 2014;40:659-672.
32. Zamora R, Srivastava AK. Controls for microgrids with storage: Review, challenges, and research needs. Renewable and Sustainable Energy Reviews. 2010;14:2009-2018.
33. Maruf A. Aminu. Validating response of ac micro-grid to three phase short circuit in grid-connected mode using dynamic analysis. International Journal of Electrical Components and Energy Conversion. 2016;2(4):21-34.
DOI: 10.11648/j.ijecec.20160204.11

Peer-review history:
The peer review history for this paper can be accessed here:
http://www.sdiarticle3.com/review-history/50762